A Subdomain Model for Armature Reaction Field and Open-Circuit Field Prediction in Consequent Pole Permanent Magnet Machines

Ahmed Abbas, Atif Iqbal

Department of Electrical Engineering, Qatar University, Qatar.

Correspondence
Ahmed Abbas, Qatar University, Department of Electrical Engineering, Qatar.
Email: ebnabass89@gmail.com

Abstract

In this paper, the machine quantity such as electromagnetic torque, self and mutual inductances, and electromotive force are analytically calculated for non-overlapping winding consequent pole slotted machine for open-circuit field and armature reaction. The sub-domain approach of (2-D) analytical model is developed using Maxwell's equations and divide the problem into slots, slot-openings, airgap and magnets region, the magnet flux-density is calculated and analyzed for both permanent magnet (PM) and armature current reaction (AR) with radial magnetization pattern. The magnetization surface currents (MSCs) are considered at the borders of iron-pole magnets and the value of MSCs is accurately computed. The result obtained using proposed model compared with that of FEM, (2-D) analytical model required less computation time and achieve higher accuracy of AR and PM.

KEYWORDS
Maxwell's equations, Permanent magnet, Torque improvement, PM machine

1 | INTRODUCTION

Slotted consequent-pole permanent magnet (CPM) machines have become attractive in some industrial applications because of their higher efficiency, higher power density and better utilization ratio [1]. In CPM the permanent magnets are magnetized in only one direction, i.e., the south poles are unchanged but the north poles have been replaced with Ferro-magnetic poles [2], [3]. Consequent-pole machines (CPM) provide scope to reduce the number of magnet material (i.e., replacing half of magnetic poles with iron poles). Therefore, CPM machines directly reduces the cost and save approximately (1/3) of amount of PM obtaining almost the same output torque compared to conventional PM machine with same specifications [4]. It has been proven that the average torque of CPM is higher than that of conventional PM machines [5].

To model the air gap saliency due to the stator slots, in [6] a 2-D analytical method presented for slotted FRPM machines based on the equivalent magnetization current (EMC). In this paper the effect of the stator slots and the effect of the rotor saliency considered. the effect of the stator slots and rotor grooves are included by injecting equivalent magnetization currents on the stator slot walls and the rotor groove edges, the PMs can be modeled by the surface currents in the lateral sidewall of the PMs [7].

Eccentric CPM has been represented in [8], investigating the electromagnetic torque and the unbalanced magnetic force. But in this paper the effect of surface magnetization currents are not calculated, therefore the effect of stator slots and groove is not included.

In [**9**], the EMC theory is used to obtain a 2-D analytical model for a slotless surface-inset PM motor; the rotor grooves are replaced by EMCs and the effect of stator slots is neglected. the rotor has a salient structure, the armature reaction effects have only been analyzed and the stator slot effects have been neglected.

To calculate flux density accurately, there are main four analytical techniques. (0-D) techniques, such as the magnetic equivalent circuit approach (MEC), is simply used to find the maximum or average value of the magnetic flux, the only drawback of this technique is the very low accuracy in case of surface-mounted magnet machines [10], [11]. It is a suitable when the effects of saturation are appeared in different parts of electrical machines. The (1-D) techniques, like lumped parameter network (LPN), is suitable when flux density consist of only one component (i.e., radial, or tangential components), as an example, when the length airgap is very small, here the tangential component can be ignored. In (2-D) techniques, the partial differential equations are derived from Maxwell's equations to compute CPM quantities [12].

(2-D) analytical model suitable candidate that gives physical insight to the machine under study and require very less computation time. Finally, the (3-D) techniques provide high accuracy, but it's not used widely because of the difficulty and complexity of deriving (3-D) equations, a (3-D) is highly time consuming specially in designing structure of PM machines. Each of the aforementioned techniques can be used either analytically or numerically.

The researchers prefer applying analytical approaches, due to their faster speed and lower computational time as compared to that of numerical approaches. One attractive applications of CPM are in-wheel drive and electric vehicles, for in-wheel, CPMs are required to satisfy some requirements: produce higher electromagnetic torque at lower speed, the ripple on torque must be low, the range of speed has to be with wide span [13], [14].

fractional slot has been produced for CPM using concentrated winding topology, these types of machines are suitable when low-speed direct drive is required due to its capability to adapt large number of magnetic poles and hence provide higher torque density with low ripple appears on torque [15], [16]. Xiaobo et al. [17] have presented a dual consequent-pole with core-tooth-to magnet configuration for both stator and rotor, it's observed that the PM flux linkage improved. CPM bearing-less motor presented by Nakagawa et al. [18], the optimal process to design CPM stator introducing magnetic suspension method to reduce magnetic saturation in the steel. Low-cost consequent-pole has been designed by Chai et al. [19] using double silent ferromagnetic iron pole. PM Vernier motors become a suitable for in-wheel applications because of its higher torque density and lower torque ripple [20], [21].

In this paper, the (2-D) model proposed in [12] is modified and extended for modelling of CPM taking into account the arc magnetization surface current (MSC). Moreover, the MSCs are considered at their exact position to have physical sense in the modelling procedure. Equivalent current theory is used to model the effects of permanent magnets (PMs). The equivalent current theory is used for surface mounted CPM. The surface magnetization currents (MSCs) are considered at the borders of iron-pole magnets and the value of MSCs is accurately computed The CPM under study is considered to be with non-overlapping winding topology and slotted stator structure. The main contributions of this paper are considering the finite permeability of cores to predict the flux density distribution in the (2-D) analytical model, finding the value of exact MSCs and also direct comparison between consequent-pole (CPM) and surface-mounted motor (SMM). All the magnets of consequent-pole PM synchronous machines (PMSMs) have the same magnetization direction. The structure of consequent-pole PM machine is shown in Figure 1.
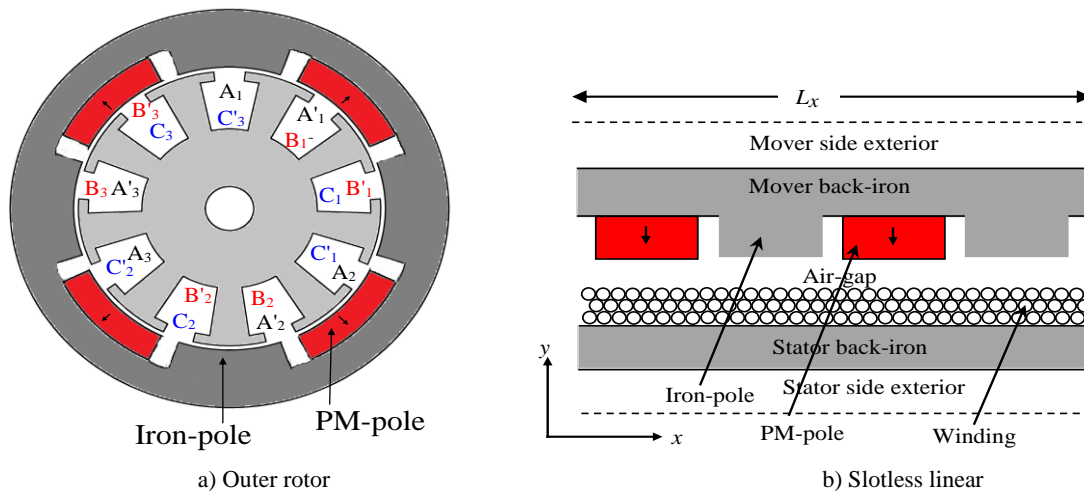

a) Outer rotor   b) Slotless linear

FIGURE 1 4 pole-pairs/ 9 slots consequent pole PMSM

2 | OVERVIEW TO THE PROPOSED SOLUTION

2.1 | Assumptions

As appeared in Figure 2, the first step is to make set assumptions for CPM under study, the main feature of making assumptions is to simplify and make analytical solution possible [22], [23]:

1) CPM considered to have infinite axial length.

2) The PMs are radially magnetized and the magnetization vector M is as $M_R\mathbf{r}.$

3) The vector of magnetic flux density and the magnetic potential are independent of $\mathbf{Z}$ i.e., $\mathbf{B} = [B_R,\ B_T,\ \mathbf{0}]$.

4) The relative permeability of PM is 1.00.

5) Infinite permeability of rotor and stator iron and the magnet poles have linear demagnetization characteristics.

6) Slot- openings and slot assumed to have radial sides.

7) Eddy current reaction field is neglected.

```
┌──────────────────────────────┐
│     Assumptions for CPM      │
└──────────────────────────────┘
               ▼
Dividing the case into a number of sub-regions
               ▼
Using of Maxwell Equations to divide The partial
deferential equation for each sub-region
               ▼
Define Boundary and Interface Conditions
               ▼
The armature current density distribution is
represented using Fourier series expansion
               ▼
Derive magnetization vector of magnets using the
Fourier series expansion.
               ▼
Finding the general solution of sub-regions
               ▼
Calculation of integration constant using the boundary
conditions
```
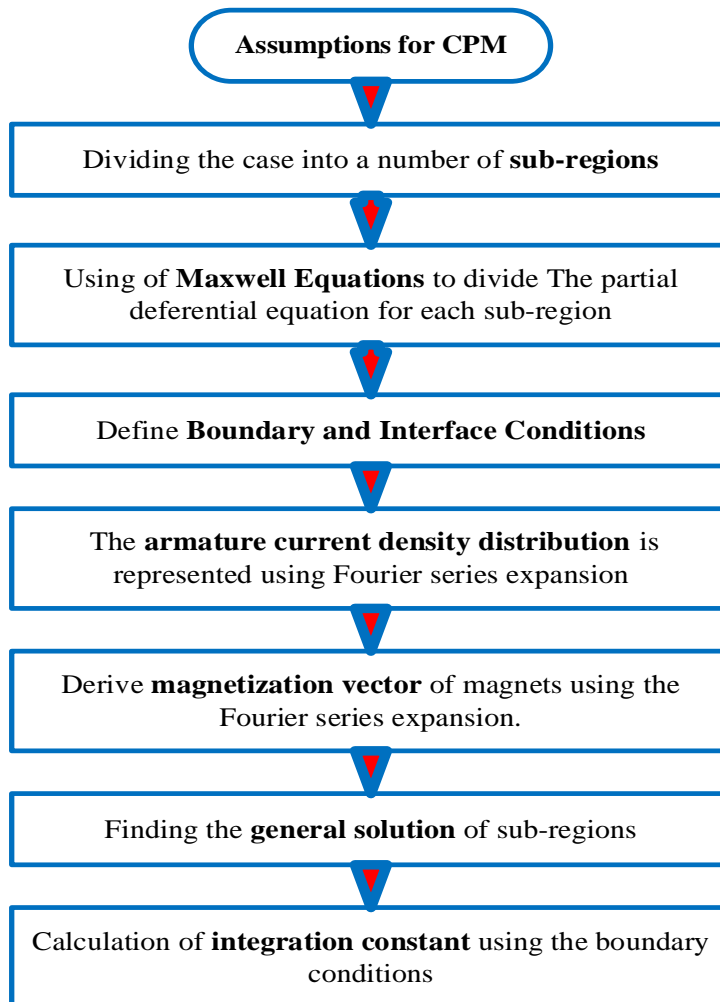
FIGURE 2   Procedure to extract CPM flux density distribution

2.2 | Magnetization Surface Currents (MSC)

The use of ferromagnetic material decreases the reluctance path of magnetic field, the reduction of the magnetic field can be explained using the concepts of magnetization volume current (MVC) and the MSC as shown below [24]:

$$J_{MVC} = \nabla \times \mathbf{M} \tag{1}$$

$$J_{MSC} = \nabla \times O_m \tag{2}$$

Where $\mathbf{M}$ is magnetization, $\mathbf{O}_m$ is unity normal vector.

According to the assumption represented in section 2.1, the resultant vector of MVC is zero. In this case some MSCs can be considered at the surface in place of ferromagnetic material, hence the MSC density can be calculated as

$$J_{MSC} = \frac{\mu_r - 1}{\mu_r \mu_o} \mathbf{B} \times O_m \simeq \frac{\mathbf{B} \times O_m}{\mu_o} = \frac{B_T}{\mu_o} \tag{3}$$

2.3 | Solution Procedure and Calculation of MSC

A shown in Figure 3, the airgap of CPM is uniform so the MSCs at the lateral borders and arcs of CPM presented as J_L and J_A respectively. To calculate MSCs, the initial MSCs considered to be zero, and the value updated at the starting of next iteration and can be expressed as,

$$J_{Lj}(r, \phi_j, \theta_r) = \frac{\pm 1}{\mu_o} B_R(r, \phi_j, \theta_r) + J_{Lj}(r, \theta_r) \tag{4}$$

The MSCs at arc can be calculated as,

$$J_A(\phi_j, \theta_r) = \frac{-1}{\mu_o} G(\phi_j) B_T(\phi_j, \theta_r) \tag{5}$$

Where $\quad G(\phi_j) = \begin{cases} 1 & \phi_{j+} < \phi < \phi_{j-} \\ 0 & elsewere \end{cases} \quad$ j=1, 2....... 2p

Figure 4 represent the flowchart for determination of resultant flux density and MSCs of CPM with few numbers of iterations.
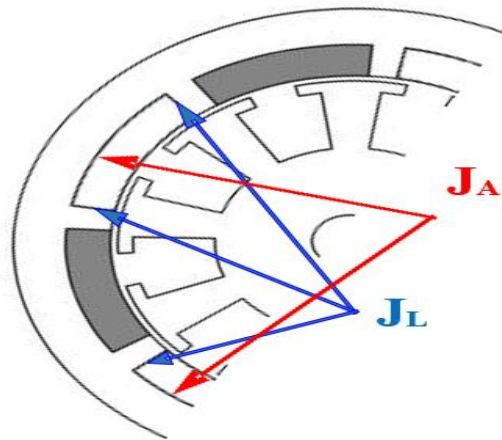

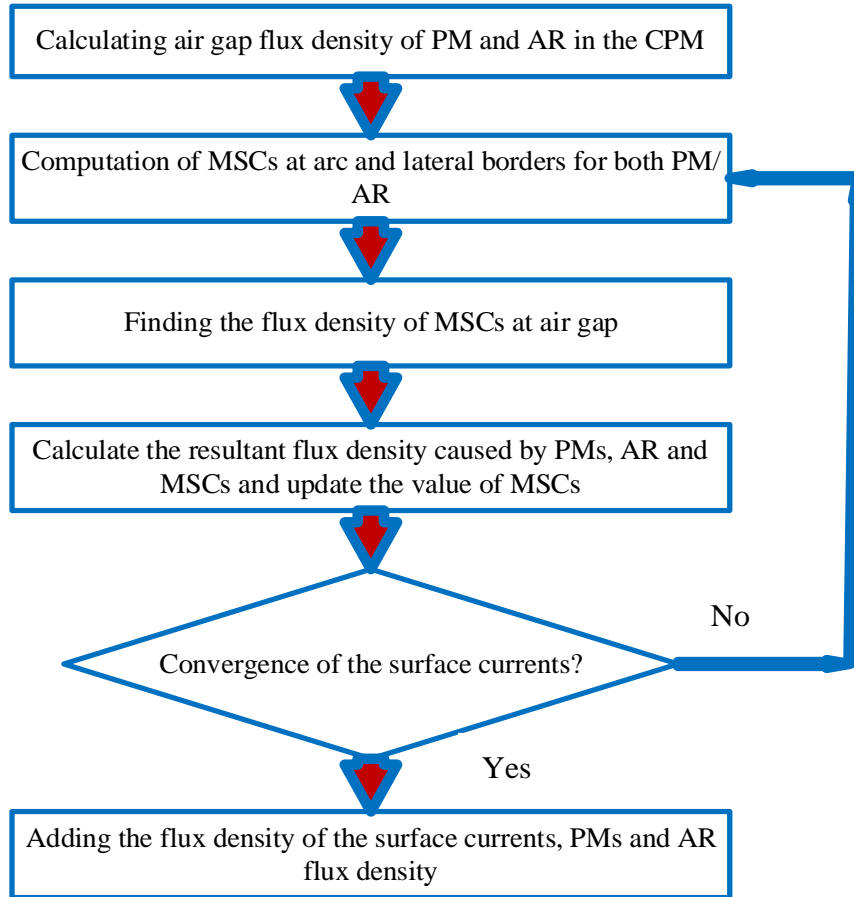FIGURE 3   Lateral and arc MSCs of CPM

```
┌─────────────────────────────────────────────────────┐
│ Calculating air gap flux density of PM and AR in the CPM │
└─────────────────────────────────────────────────────┘
                          ↓
┌─────────────────────────────────────────────────────┐
│ Computation of MSCs at arc and lateral borders for both PM/ │
│ AR                                                   │
└─────────────────────────────────────────────────────┘
                          ↓
┌─────────────────────────────────────────────────────┐
│ Finding the flux density of MSCs at air gap          │
└─────────────────────────────────────────────────────┘
                          ↓
┌─────────────────────────────────────────────────────┐
│ Calculate the resultant flux density caused by PMs, AR and │
│ MSCs and update the value of MSCs                    │
└─────────────────────────────────────────────────────┘
                          ↓
              ◇ Convergence of the surface currents? ◇ — No
                          ↓ Yes
┌─────────────────────────────────────────────────────┐
│ Adding the flux density of the surface currents, PMs and AR │
│ flux density                                         │
└─────────────────────────────────────────────────────┘
```

FIGURE 4   The method used to compute flux density

2.3 | GOVERNING PARTIAL DEFERENTIAL EQUATION (PDEs)

By considering magnetic vector potential and applying Maxwell equations to CPM, the general solution of the proposed machine is derived and expressed for each of the CPM regions, i.e., slot (St), magnets (Mg), air gap (ag), and slot opening (So).

A methodology for study the problem resolution for magnetism is presented by Ampere's law $\nabla . \boldsymbol{B} = 0$ and Gauss's law $\nabla \times \boldsymbol{H} = \boldsymbol{J}$, wherein $\boldsymbol{H}$ is the magnetic intensity vector and $\boldsymbol{J}$ is the vector of electric current density. The corresponding relationship between magnetic field density vector and intensity vector is expressed as follow:

$$\boldsymbol{B} = \mu_0 \mu_r \boldsymbol{H} + \mu_0 \boldsymbol{M} \tag{6}$$

Where μ_0 is the free space permeability, μ_r is the relative permeability and $\boldsymbol{M}$ is the magnetization vector in A/m. Using (1) in Ampere's circuital law, we can get:

$$\nabla \times \boldsymbol{B} = \mu_0 \mu_r \nabla \times \boldsymbol{H} + \mu_0 \nabla \times \boldsymbol{M} \tag{7}$$

According to gauss's law, flux density is determined as follow:

$$\boldsymbol{B} = \nabla \times \boldsymbol{A} \tag{8}$$

With substituting (7) into (8) and considering $\nabla . \boldsymbol{A} = 0$, governing equation is achieved as follow:

$$\nabla^2 \boldsymbol{A} = -\mu_0 \mu_r \boldsymbol{J} - \mu_0 \nabla \times \boldsymbol{M} \tag{9}$$

By the use of separated variables technique, the general solution of CPM using Laplace and Poisson equation for all regions

can be obtained.

$$\nabla^2 \boldsymbol{A}^w = -\mu_0 \boldsymbol{J} \tag{10}$$

$$\nabla^2 \boldsymbol{A}^m = -\mu_0 \nabla \times \boldsymbol{M} \tag{11}$$

$$\nabla^2 \boldsymbol{A}^i = 0 \tag{12}$$

Where superscripts (*w, m*) designate the winding and magnet, respectively and (*i*) is representative of other regions such as airspace, slot and slot-opening regions

2.4 | ARMATURE REACTION AND FLUX DENSITY

Considering CPM with symmetrical winding, the 3-phase armature current can be expressed by the following Fourier series,

$$i_j(t) = \sum_u I_m \sin[u(pwt - \gamma_j) + \theta_m] \quad \text{j=1, 2, 3} \tag{13}$$

Where (I_m and θ_m) are respectively, the amplitude and phase shift of the ***u***-th harmonic of the phase current. And $\gamma_j = 2\pi(j-1)/q$ is the phase angle of phase ***j*** with respect to the first phase and ***w*** represent the velocity of the rotor.

The current density distribution of a 3-phase winding expressed by the following equation:

$$J(\theta, t) = \sum_u J_s(t) \sin(np\theta) + J_c(t) \cos(np\theta) \tag{14}$$

Where

$$J_s(t) = \sum_{j=1}^{q} \frac{4 \, pN_t}{\pi |R_s^2 - R_a^2|} k_{pm} k_{dm} i_j(t) \cos(n\delta_j) \tag{15}$$

$$J_c(t) = -\sum_{j=1}^{q} \frac{4 \, pN_t}{\pi |R_s^2 - R_a^2|} k_{pm} k_{dm} i_j(t) \sin(n\delta_j) \tag{16}$$

$$k_{pm} = \sin\left(\frac{n\theta_c}{2}\right) \, \& \, k_{dm} = \frac{\sin(n\pi/2q)}{n\pi/2q} \tag{17}$$

In (2-D) analytical approach considering polar coordinates coordinate, the magnetization vector has only radial and tangential components as follows,

$$M = M_R r + M_T \theta$$

Where ***r*** the radial unit vector and ***θ*** is the tangential unit vector. M_R and M_T are the component of radial and tangential magnetization vector, these vectors can be expressed by Fourier series as:

$$M_R^k(\theta) = \sum_{w=1,3,5......}^{W} M_{Rw}^k \sin(\frac{wp}{\alpha_r}(\theta - \alpha - \frac{2k\pi}{p} + \frac{\alpha_r \pi}{2p})) \tag{18}$$

$$M_T^k(\theta) = \sum_{w=1,3,5......}^{W} M_{Tw}^k \cos(\frac{wp}{\alpha_r}(\theta - \alpha - \frac{2k\pi}{p} + \frac{\alpha_r \pi}{2p})) \tag{19}$$

Where ***α*** is the angle position of the rotor, $\boldsymbol{\alpha_r}$ is the rotor iron arc per pole pitch ratio. In the proposed model we use radial magnetization patterns, as shown in Figure 5, illustrate the radial magnetization pattern used in this and can be defined by the following expressions:

$$\left. \begin{array}{l} M_{Rw} = \frac{4 \, B_{rem}}{\mu_o w\pi} \sin\left(\frac{w\pi\alpha_p}{2\alpha_r}\right) \\ M_{Tw} = 0 \end{array} \right\} \tag{20}$$

Where α_p the pole arc per pole pitch ratio, and B_{rem} is the remanence flux density of the magnet.
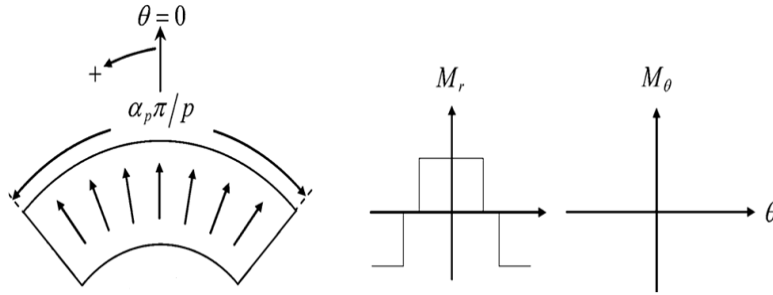

FIGURE 5   Radial and Tangential Magnetization pattern of CPM

2.5| Obtaining Integral Coefficient

The boundary/interfacing conditions are applied on CPM based on the reality that the components of the magnetic flux density are continuous between any two regions. Due to complexity of represented the integral constants in a simple closed form, hence numerical calculations are used at this stage.

By applying the boundary conditions listed in Table I of Appendix A and considering the correlation approach, the integral constants are obtained and expressed in matrix form as shown in Appendix B.

Using the general solution of the magnetic vector potential listed in Table II of Appendix A, the radial and tangential components of flux density for the airgap, arc MSCs and lateral MSCs can be calculated as,

$$B_R^a(r,\theta) = -\sum_{n=1}^{N} n\left\{\left[\frac{a_n^a}{R_s}\left(\frac{r}{R_s}\right)^{n-1} + \frac{b_n^a}{R_m}\left(\frac{R_m}{r}\right)^{n+1}\right]\sin(n\theta) - \left[\frac{c_n^a}{R_s}\left(\frac{r}{R_s}\right)^{n-1} + \frac{d_n^a}{R_m}\left(\frac{R_m}{r}\right)^{n+1}\right]\cos(n\theta)\right\} \quad (21)$$

$$B_T^a(r,\theta) = -\sum_{n=1}^{N} n\left\{\left[\frac{a_n^a}{R_s}\left(\frac{r}{R_s}\right)^{n-1} - \frac{b_n^a}{R_m}\left(\frac{R_m}{r}\right)^{n+1}\right]\cos(n\theta) - \left[\frac{c_n^a}{R_s}\left(\frac{r}{R_s}\right)^{n-1} + \frac{d_n^a}{R_m}\left(\frac{R_m}{r}\right)^{n+1}\right]\sin(n\theta)\right\} \quad (22)$$

$$B_R^{arc}(r,\theta) = \sum_{n=1,}^{N} Y_n\left(r^{np+1} + R_s^{2np}r^{-np-1}\right)\left(J_{snArc}\cos(np(\theta-\theta_r)) - J_{cnArc}\sin(np(\theta-\theta_r))\right) \quad (23)$$

$$B_T^{arc}(r,\theta) = \sum_{n=1,}^{N} Y_n\left(R_s^{2np}r^{-np-1} - r^{np-1}\right)\left(J_{snArc}\sin(np(\theta-\theta_r)) + J_{cnArc}\cos(np(\theta-\theta_r))\right) \quad (24)$$

$$B_R^{Lat}(r,\theta) = \sum_{n=1,}^{N} C_n\left(r^{np+1} + R_s^{2np}r^{-np-1}\right)\left(J_{snLat}\cos(np(\theta-\theta_r)) - J_{cnLat}\sin(np(\theta-\theta_r))\right) \quad (25)$$

$$B_T^{Lat}(r,\theta) = -\sum_{n=1,}^{N} C_n\left(r^{np-1} - R_s^{2np}r^{-np-1}\right)\left(J_{snLat}\sin(np(\theta-\theta_r)) - J_{cnLat}\cos(np(\theta-\theta_r))\right) \quad (26)$$

Where

$$Y_n = \mu_o R_m \frac{R_m^{np} + R_s^{np}\left(\frac{R_s}{R_m}\right)^{np}}{2(R_r^{np} - R_s^{2np})}$$

$$C_n = \mu_o R_m \frac{2\mu_o\left(R_m^{np} - R_s^{2np}R_m^{-np}\right)}{2np(4-(np)^2)(R_r^{2np} - R_s^{2np})}\left[\frac{-R_s^{np+2}R_m^{-np} + R_m^2}{R_m^{np} - R_s^{2np}R_m^{-np}} - R_s^{np+2}\right]$$

3 | MACHINE QUANTITIES

3.1| Self and Mutual Inductance

The self and mutual inductance of CPM computed is after calculation of flux density distribution due to only the armature reaction current. Following equation represent the mutual inductance between phase j and *m:*

$$L_{jk} = \frac{\emptyset_{j,m}}{ij} \tag{27}$$

Using same procedure, the self-inductance can be calculated when j=m, $\emptyset_{j,m}$ is the flux linkage. Assuming a q-phase with a symmetrical winding, the magnetic flux linked by m-th coil of the j-th phase can be expressed as:

$$\emptyset_{j,k}(\alpha) = R_w L_s \int_{-\frac{\theta_c}{2p}+\delta_{j,k}}^{\frac{\theta_c}{2p}+\delta_{j,k}} \boldsymbol{B_R}\ (R_w, \theta' - \alpha) d\theta' \tag{28}$$

Where $\boldsymbol{B_R}$ is the radial component of flux density of phase current and resultant of MSCs $\delta_{j,k} = 2\pi(k-1)/p$ Is the phase shift.

3.2 | Back -emf

The total back-EMF induced in phase j, can be analytically found using Faraday's law as shown below:

$$E_j = -pN_t\omega \frac{d\emptyset_{j,k}}{d\alpha} \tag{29}$$

Where Nt is the number of turns/coils, α is the angular position of the rotor and $\emptyset_{jm}$ is the magnetic flux linkage between the coils.

3.3 | Instantaneous Electromagnetic Torque

Calculation of torque require both the open circuit filed and armature reaction, instantaneous torque mainly consist of cogging torque, electromagnetic torque and reluctance torque.

$$T(t) = T_{cog}(t) + T_{em}(t) + T_{rel}(t) \tag{30}$$

Based on Maxwell's theory:

$$T(t) = \frac{L_s R_C^2}{\mu} \int_0^{2\pi} \boldsymbol{B_R}\ (r, \phi, \theta_r) \boldsymbol{B_T}(r, \phi, \theta_r)\ d\phi \tag{31}$$

The electromagnetic torque in the case under study developed due to the interaction of AR with MSCs and PMs located on the rotor.

3.4 | Unbalance Magnetic Force

UMF consist of radial and tangential components, based on Maxwell stress tensor approach, the radial and tangential components of the magnetic local traction acting on each rotor surface can be obtained as

$$F_R(t) = L \int_{-\Pi}^{\Pi}(f_R\cos\theta - f_T\sin\theta)\, rd\theta \tag{32}$$

$$F_T(t) = L \int_{-\Pi}^{\Pi}(f_R\sin\theta + f_T\cos\theta)\, rd\theta \tag{33}$$

Where

$$f_R = \frac{1}{2\mu_o}(B_R^2 - B_T^2) \quad \& \quad f_T = \frac{1}{\mu_o}(B_R B_T) \tag{34}$$

The magnitude of the unbalanced force can be obtained as

$$|F| = \sqrt{(F_R^2(t) + F_T^2(t))} \qquad (35)$$

The above equation applied to compute the UMF originating from the magnet if ($B_R^a = B_{R,PM}^a$ & $B_T^a = B_{T,PM}^a$), the UMF from the armature reaction current if ($B_R^a = B_{R,AR}^a$ & $B_T^a = B_{T,AR}^a$) and the total UMF if ($B_R^a = B_{R,AR}^a + B_{R,PM}^a$ & $B_T^a = B_{T,AR}^a + B_{T,PM}^a$)

3.5 | Result Verification

Consequent-pole PMs can be developed by replacing the S magnet poles in the surface-mounted motor with iron poles results in an increased interaction between the iron and PMs Therefore, the cogging torque is increased in the consequent-pole motor. The value of calculated MSCs of lateral and arc of iron poles are presented in Figure 6 and Figure 7 at $\theta_r = 45°$ it's clearly observed that the MSCs increases the airgap flux density.

The parameters used in this study (non-overlapping windings slotted CPM) listed in Table III. To ensure satisfactory accuracy of the result, the number of harmonics in slot, slot-opening, air gap and PMs is considered to be ($(S_h) = (So_h) = (ag_h) = (PM_h) = 100$). By applying three phases sinusoidal current with amplitude of 10.55A with frequency of 100 Hz, the component of calculated flux density (radial and tangential components) due to AR and PMs are, respectively ($B_{R,PM}^a, B_{T,PM}^a$ & $B_{R,AR}^a, B_{T,AR}^a$), obtained as shown in Figure 7,8 and Figure 9, 10 respectively.
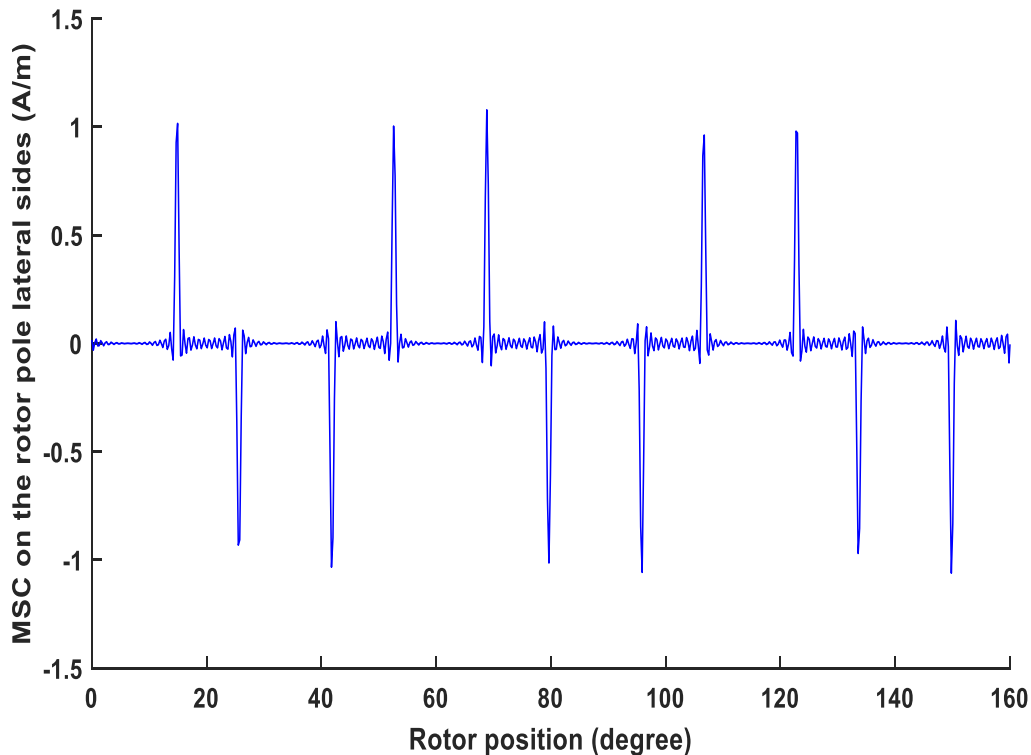

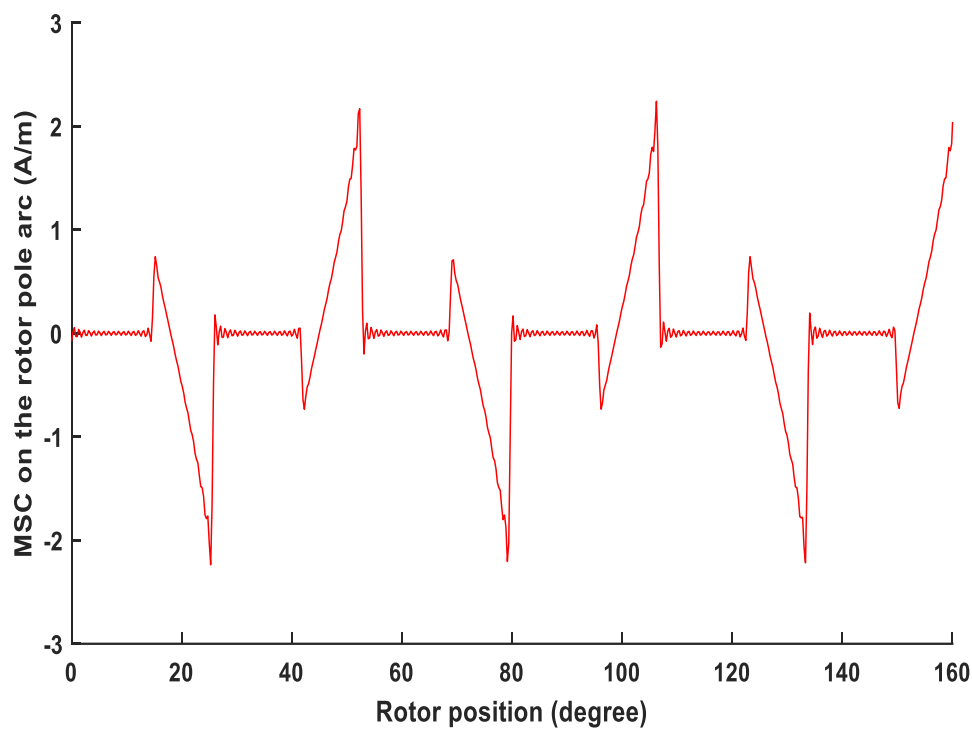FIGURE 6 Lateral current density.
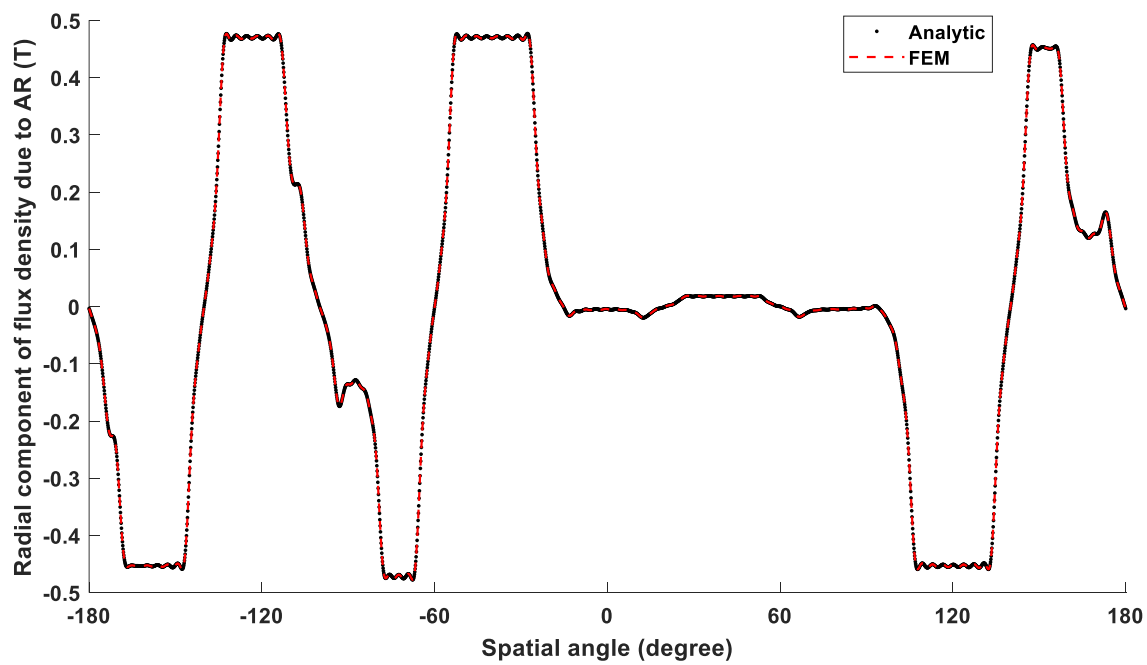
FIGURE 7 Arc current density.

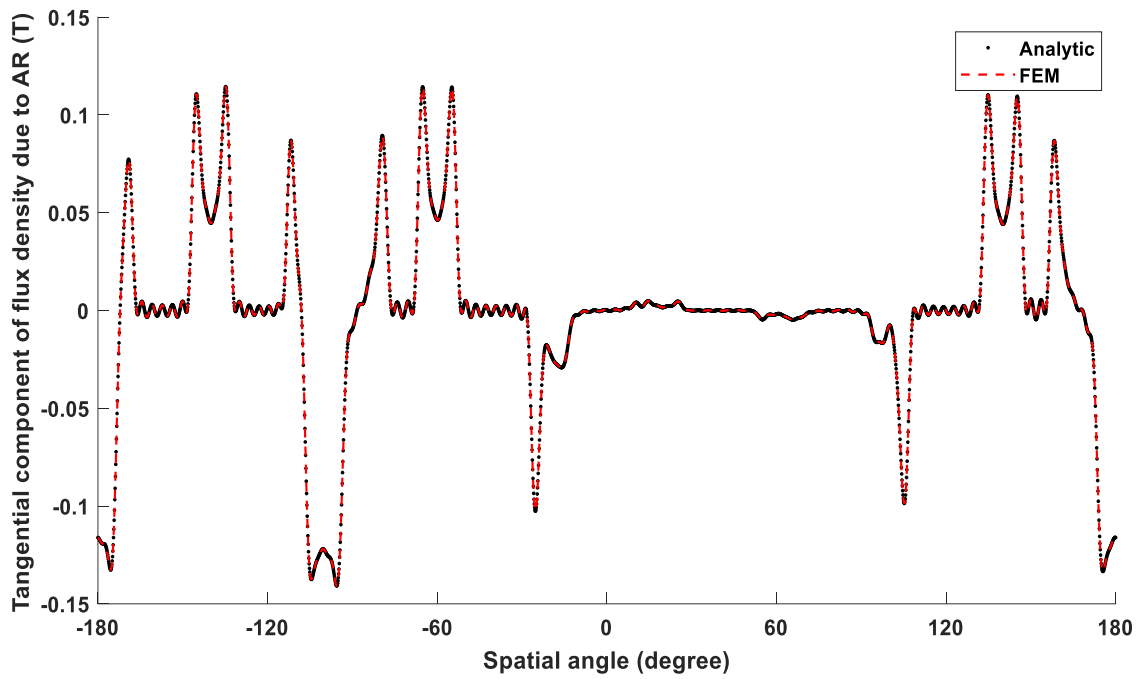FIGURE 8 Radial Component of flux density due to armature reaction

FIGURE 9 Tangential Component of flux density due to armature reaction
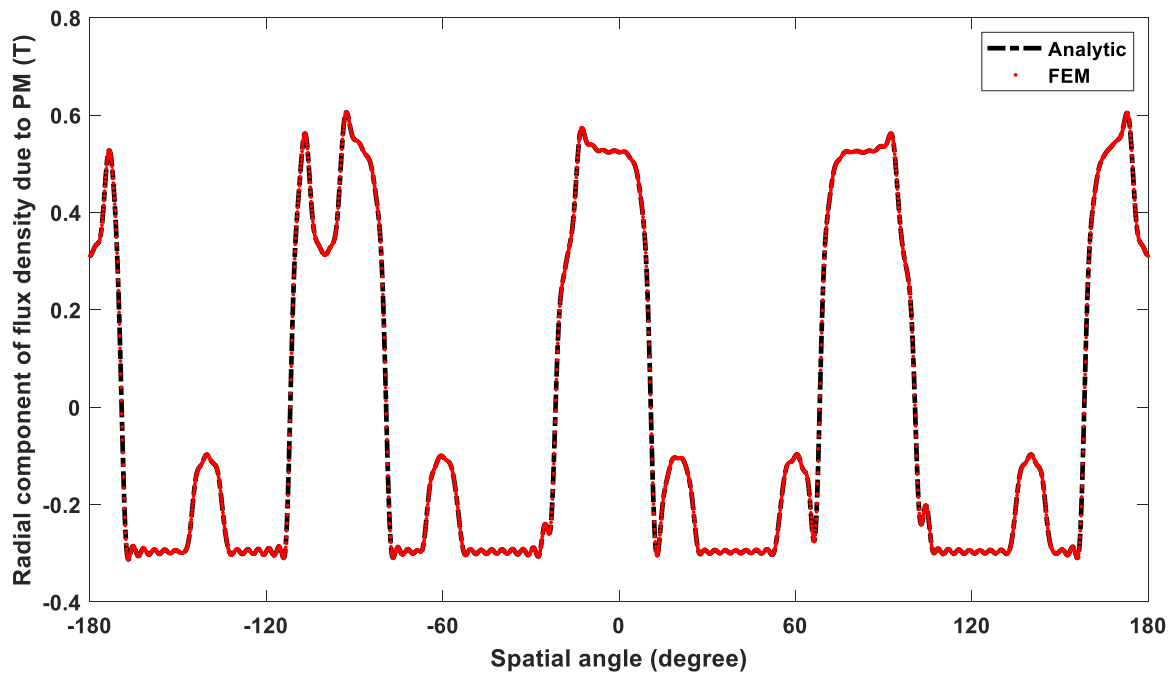

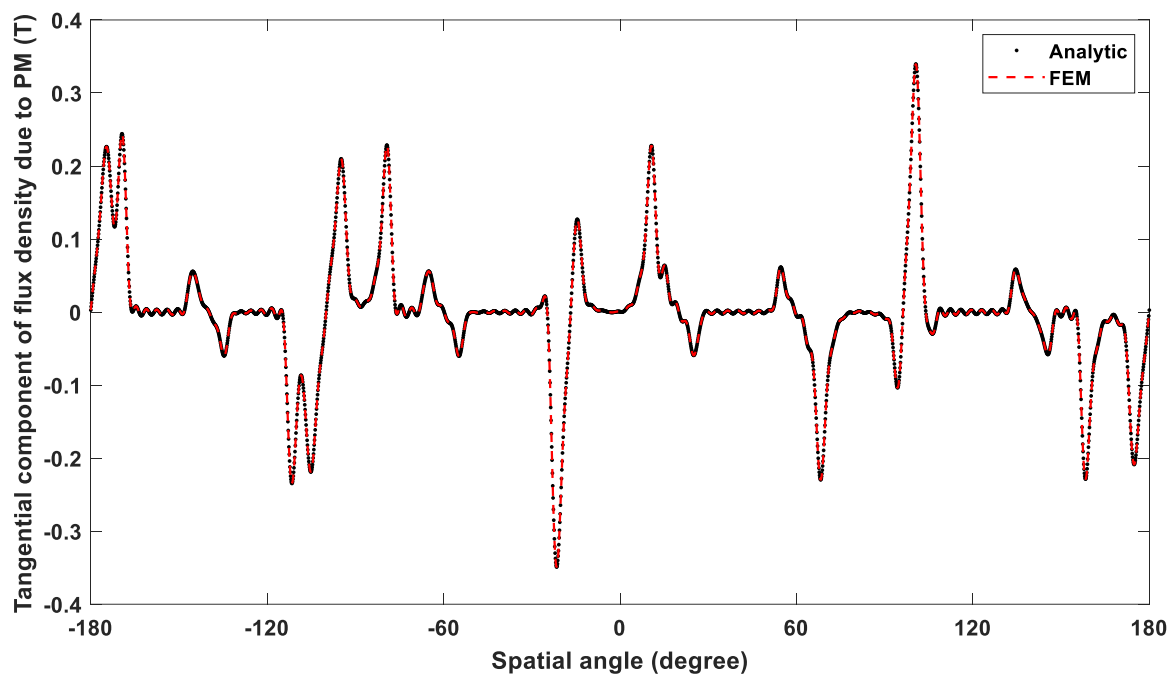FIGURE 10 Radial component of flux density due to permanent magnet

FIGURE 11 Tangential component of flux density due to permanent magnet
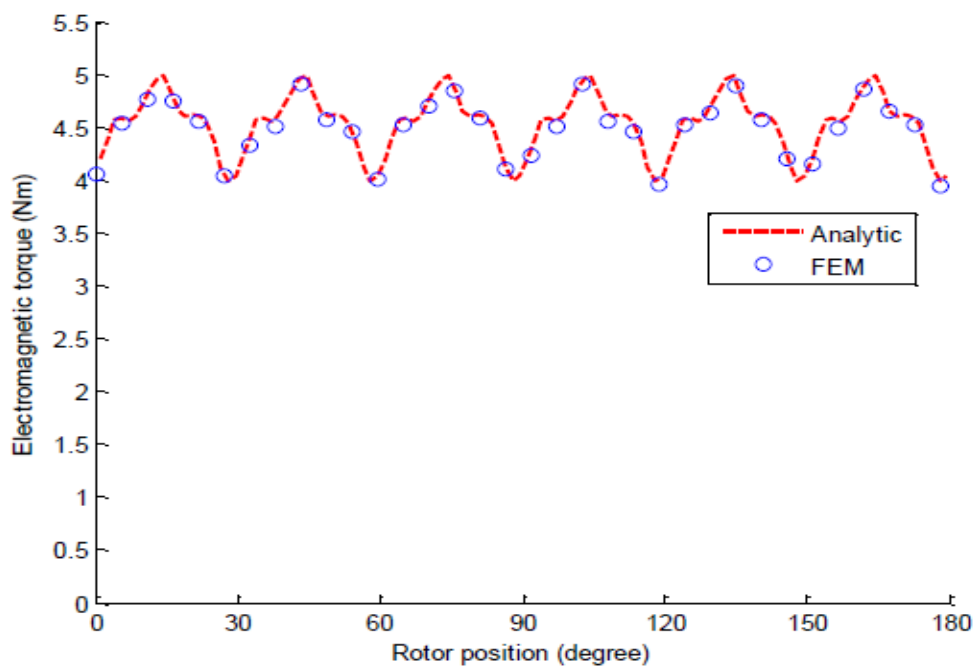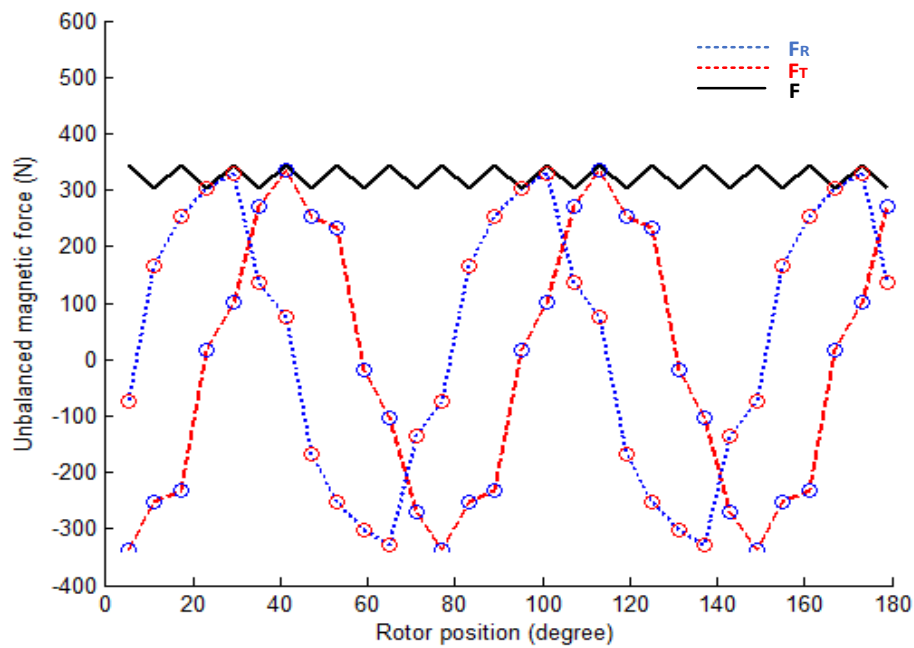

FIGURE 12 Electromagnetic Torque
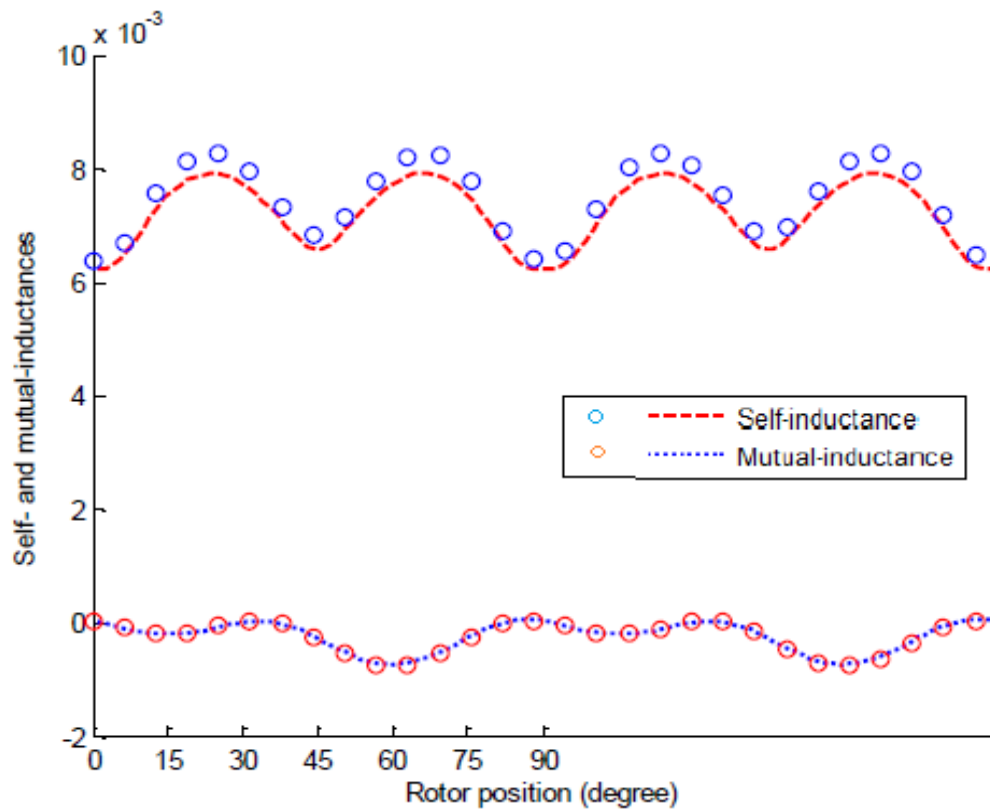
FIGURE 13 Unbalanced magnetic forces.

FIGURE 14 Self and mutual inductances of CPM

The computation of electromagnetic torque and unbalanced magnetic forces mainly require the flux density result from both permanent magnet field and armature reaction. The electromagnetic torque of the case under study and unbalance magnetic force (UMF) represented in Figure 12 & Figure 13. The self- and mutual inductance is depicted in Figure. 14.

In a comparison to surface-mounted motor, consequent pole motor iron losses are very low and lower inductance due to the small airspace and hence lower magnetic reluctance. The replacement of S-poles in surface-motor with iron in CPM results in an increased interaction between the iron part and permanent magnets. Therefore, its observed that the cogging torque is increased in CPM. The cost of CPM is reduced to the half due to elimination of half of PMs, Table IV compares the performance of the CPM motor with surface-mounted motor.

TABLE IV   Comparison between Consequent-Pole and Surface-Mounted motor

Quantities	CPM	SMM
Maximum radial flux density (T)	1.03	1.14
Maximum tangential flux density (T)	0.41	0.48
The induced voltage in phase (Vrms)	41.4	45.7
Electromagnetic torque (Nm)	6.25	8.21
Maximum cogging torque (Nm)	0.15	0.013
Maximum reluctance torque (Nm)	0.11	0
Maximum self-inductance (mH)	3.2	1.8
Minimum self-inductance (mH)	2	1.8
Copper loss (W)	162	162
Core loss (W)	13.0	17.5
P_{out} (W)	981	1289
Efficiency (%)	84.9	87.8

4 | CONCLUSION

In this study, analytical model using (2-D) sub-domain technique to magnetic field problem of CPM equipped with stator slots and non-overlapping winding has been developed. The performance of case under study has been performed by calculating the flux density distribution due to both permanent magnets and armature reaction. The analytical expression and CPM quantities has been tested on (4 pol-pairs/ 9 slots) with radial magnetization pattern and sinusoidal input current, the generated expressions can be used for any CPM with any combination of poles, slots number and any magnetization patterns. The MSCs currents of lateral and arc borders of the CPM has been computed, its observed that MSCs increased the airgap flux density. The CPM quantities calculated and analyzed using (2-D) approach and compared with that of FEM.

AKNOWLEDGMENT

REFERENCES

1. Jun Amemiya, Akira Chiba, David G. Dorrell and Tadashi Fukao, "Basic Characteristics of a Consequent-Pole-Type Bearingless Motor," *IEEE Transactions on Magnetics*, vol. 41, no. 1, 2005.

2. Y. Ueda, H. Takahashi, T. Akiba and M. Yoshida, "Fundamental Design of a Consequent-Pole Transverse-Flux Motor for Direct-Drive Systems," in IEEE Transactions on Magnetics, vol. 49, no. 7, pp. 4096-4099.

3. S. Teymoori, A. Rahideh, H. Moayed-Jahromi, and M. Mardaneh, "Two-dimensional analytical magnetic field prediction for consequent-pole permanent magnet synchronous machines," *IEEE Trans. Magn.*, vol. 52, no.

4. S. U. Chung, J. W. Kim, Y. D. Chun, B. C. Woo, and D. K. Hong, "Fractional slot concentrated winding PMSM with consequent-pole rotor for a low-speed direct drive: reduction of rare earth permanent magnet," IEEE Transactions on Energy Conversion, vol. 30, no. 1, pp. 103–109, Mar. 2015.

5. B. Ren, G. Li, Z. Q. Zhu, M. Foster, and D. Stone, "Performance comparison between consequent-pole and inset modular permanent magnet machines," The Journal of Engineering, vol. 2019, no. 17, pp. 3951-3955, Jun. 2019.

6. S. T. Boroujeni and V. Zamani, "A novel analytical model for no-load, slotted, surface-mounted PM machines: Air gap flux density and cogging torque," *IEEE Trans. Magn.*, vol. 51, no. 4, Apr. 2015, Art. no. 8104008.

7. V. Zamani, A. Rahideh, M. Mardaneh, S.Taghipour "Analytical Modeling of Flux-Reversal Permanent-Magnet Machines," *IEEE Trans. Energy Convers.*, vol. 36, no. 2, June. 2021.

8. S Taghipour Boroujeni, SP Emami, N Takorabet, A Mahmoudi, "Analytical investigation of the armature current influence on the torque and radial force in eccentric consequent-pole PM machines,"IET Electric Power Applications 11 (3), 312-322.

9. S. T. Boroujeni and H. B. Naghneh, "Analytical modeling and prototyping a slotless surface-inset PM machines," *IET Electric Power Appl.*, vol. 11, no. 3, Mar. 2017, pp. 312–322.

10. H. Dhulipati, S. Mukundan, Z. Li, E. Ghosh, J. Tjong and N. C. Kar, "Torque Performance Enhancement in Consequent Pole PMSM Based on Magnet Pole Shape Optimization for Direct-Drive EV," in IEEE Transactions on Magnetics, vol. 57, no. 2, pp. 1-7, Feb. 2021.

11. A. Ghaffari, A. Rahideh, H. Moayed-Jahromi, A. Vahaj, A. Mahmoudi and W. L. Soong, "2-D Analytical Model for Outer-Rotor Consequent-Pole Brushless PM Machines," in IEEE Transactions on Energy Conversion, vol. 34, no. 4, pp. 2226-2234, Dec. 2019.

12. M. Wang, X. Qiu, J. Yang, X. Chen and Y. Dou, "Study on the Electromagnetic Characteristics of the Consequent Pole In-Wheel Motor," 2016 IEEE Vehicle Power and Propulsion Conference (VPPC), 2016, pp. 1-5.

13. Y. Gao, R. Qu, D. Li, J. Li and G. Zhou, "Consequent-Pole Flux-Reversal Permanent-Magnet Machine for Electric Vehicle Propulsion," in IEEE Transactions on Applied Superconductivity, vol. 26, no. 4, pp. 1-5, June 2016.

14. R. Zhou, G. J. Li, Z. Q. Zhu, Y. X. Li, M. P. Foster and D. A. Stone, "Investigation of Integer/Fractional Slot Consequent Pole PM Machines with Different Rotor Structures," 2019 IEEE International Electric Machines & Drives Conference (IEMDC), 2019, pp. 119-126.

15. S. Cai, Z. -Q. Zhu, C. Wang, J. -C. Mipo and S. Personnaz, "A Novel Fractional Slot Non-Overlapping Winding

Hybrid Excited Machine with Consequent-Pole PM Rotor," in IEEE Transactions on Energy Conversion, vol. 35, no. 3, pp. 1628-1637, Sept. 2020.

16. X. Yang, B. Kou, J. Luo and H. Zhang, "A Novel Dual-Consequent-Pole Transverse Flux Motor and Its Analytical Modeling," in IEEE Transactions on Industrial Electronics, vol. 68, no. 5, pp. 4141-4152, May 2021.

17. M. Nakagawa et al., "Optimization of Stator Design in a Consequent-Pole Type Bearingless Motor Considering Magnetic Suspension Characteristics," 2006 IEEE International Magnetics Conference (INTERMAG), 2006, pp. 195-195.

18. W. Chai, Z. Cai, B. -I. Kwon and J. -W. Kwon, "Design of a Novel Low-Cost Consequent-Pole Permanent Magnet Synchronous Machine," in IEEE Access, vol. 8, pp. 194251-194259, 2020.

19. Y. Yu, Y. Pei, L. Chen, F. Chai and G. Han, "Design and Comparative Analysis of Consequent Pole Rotor Configurations in PM Vernier Motors for In-wheel Drive Application," 2019 22nd International Conference on Electrical Machines and Systems (ICEMS), 2019, pp. 1-6.

20. H. Zhou, W. Tao, C. Zhou, Y. Mao, G. -J. Li and G. Liu, "Consequent Pole Permanent Magnet Vernier Machine With Asymmetric Air-Gap Field Distribution," in IEEE Access, vol. 7, pp. 109340-109348, 2019.

21. C. Shi, D. Li, R. Qu, H. Zhang, Y. Gao and Y. Huo, "A Novel Linear Permanent Magnet Vernier Machine With Consequent-Pole Permanent Magnets and Halbach Permanent Magnet Arrays," in IEEE Transactions on Magnetics, vol. 53, no. 11, pp. 1-4, Nov. 2017.

22. H. Moayed-Jahromi, A. Rahideh and M. Mardaneh, "2-D Analytical Model for External Rotor Brushless PM Machines," in IEEE Transactions on Energy Conversion, vol. 31, no. 3, pp. 1100-1109, Sept. 2016.

23. A. Rahideh and T. Korakianitis, "Analytical Magnetic Field Calculation of Slotted Brushless Permanent-Magnet Machines With Surface Inset Magnets," in IEEE Transactions on Magnetics, vol. 48, no. 10, pp. 2633-2649, Oct. 2012.

24. S. Taghipour Boroujeni and V. Zamani, "A Novel Analytical Model for No-Load, Slotted, Surface-Mounted PM Machines: Air Gap Flux Density and Cogging Torque," in *IEEE Transactions on Magnetics*, vol. 51, no. 4, pp. 1-8, April 2015, Art no. 8104008.

APPENDIX A

TABLE I The Boundary Conditions of CPM

Region 1	Region 2	Boundary	Interface	Range
Magnet k	Rotor iron	$H_T^{m,k}(r,\theta) = 0$	$r = R_r$	$\left\|\theta - \alpha - \dfrac{2k\pi}{p}\right\| \leq \dfrac{\alpha_r \pi}{2p}$
Magnet k	Both sides iron-pole	$H_R^{m,k}(r,\theta) = 0$	$\theta = \alpha - \dfrac{2k\pi}{p} \pm \dfrac{\alpha_r \pi}{2p}$	$R_r \leq r \leq R_m$
Air-gap	Magnet k	$B_R^a(r,\theta) = B_R^{m,k}(r,\theta)$	$r = R_m$	$\left\|\theta - \alpha - \dfrac{2k\pi}{p}\right\| \leq \dfrac{\alpha_r \pi}{2p}$
Air-gap	Magnets & iron-poles	$H_T^a(r,\theta) = \begin{cases} \displaystyle\sum_{k=0}^{p-1} H_T^{m,k}(r,\theta) \\ 0 \end{cases}$	$r = R_m$	$\begin{cases} \left\|\theta - \alpha - \dfrac{2k\pi}{p}\right\| \leq \dfrac{\alpha_r \pi}{2p} \\ else\ where \end{cases}$
Slot-opening j	Both sides tooth-tip	$H_T^{so,j}(r,\theta) = 0$	$\theta = \theta_j \pm \beta$	$R_s \leq r \leq R_{so}$
Air-gap	Slot-opening j	$B_R^a(r,\theta) = B_R^{so,j}(r,\theta)$	$r = R_s$	$\begin{cases} \theta_j - \dfrac{\delta}{2} \leq \theta < \theta_j - \dfrac{\beta}{2} \\ \theta_j - \dfrac{\delta}{2} \leq \theta \leq \theta_j - \dfrac{\beta}{2} \\ \theta_j - \dfrac{\delta}{2} < \theta \leq \theta_j - \dfrac{\beta}{2} \end{cases}$
Air-gap	Slot-openings & teeth	$H_T^a(r,\theta) = \begin{cases} \displaystyle\sum_{j=0}^{Q} H_T^{so,j}(r,\theta) \\ 0 \end{cases}$	$r = R_s$	$\|\theta - \theta_j\| \leq \dfrac{\beta}{2}$
Slot j	Slot-opening j	$B_R^{sl,j}(r,\theta) = B_R^{so,j}(r,\theta)$	$r = R_{so}$	$\begin{cases} \|\theta - \theta_j\| \leq \dfrac{\beta}{2} \\ else\ where \end{cases}$
Slot j	Tooth-tip Slot-opening j Tooth-tip	$H_T^{sl,j}(r,\theta) = \begin{cases} 0 \\ H_T^{so,j}(r,\theta) \\ 0 \end{cases}$	$r = R_{so}$	$\|\theta - \theta_j\| \leq \dfrac{\beta}{2}$
Slot j	Both sides tooth	$H_R^{sl,j}(r,\theta) = 0$	$\theta = \theta_j \pm \delta_j$	$R_s \leq r \leq R_{so}$
Slot j	Stator back-iron	$H_T^{sl,j}(r,\theta) = 0$	$r = R_{sl}$	$\|\theta - \theta_j\| \leq \dfrac{\delta}{2}$

For m=0, 1……(*p*-1), **p** represents the number of PMs.

For j=1,….*S* where *S* is the number of slots in stator slots $\theta_j = 2\pi(j - 0.5)/Q$ is the angle of the center of slot *j* w.r.t. x-axis.

Where δ and β are the span angles of the slot and slot-opening respectively, $\alpha = wt + \alpha_0$ is the rotor angular position, is the rotor rotational velocity, α_0 is the initial position of the rotor and α_r is the iron groove of the rotor to pole-pitch ratio.

TABLE II The General Solution of All Sub-regions of CPM

Regions	General solutions	Integral constants
Magnet k	$A_z^{m,k}(r,\theta) = \sum_{w=1}^{W} \left\{ a_w^{m,k}\left[\left(\frac{r}{R_m}\right)^{\bar{w}} + \left(\frac{R_r}{R_m}\right)^{\bar{w}}\left(\frac{R_r}{r}\right)^{\bar{w}}\right] + R_r\xi_{w1}^k\left(\frac{R_r}{r}\right)^{\bar{w}} + k_w^k r \right\}\cos(\bar{w}(\theta - \alpha - \frac{2k\pi}{p} + \frac{\alpha_r\pi}{2p}))$	$a_w^{m,0},\ldots\ldots,a_w^{m,p-1}$ For w=1,……,W
Air-gap	$A_z^a(r,\theta) = \sum_{n=1}^{N}\left[a_n^a\left(\frac{r}{R_s}\right)^{\bar{n}} + b_n^a\left(\frac{R_m}{r}\right)^n\right]\cos(n\theta) + \left[c_n^a\left(\frac{r}{R_s}\right)^{\bar{n}} + d_n^a\left(\frac{R_m}{r}\right)^n\right]\sin(n\theta)$	$a_n^a, b_n^a, c_n^a, d_n^a$ For n=1,……….,N
Slot-openings j	$A_z^{so,j}(r,\theta) = b_0^{so,j}\ln r + \sum_{u=1}^{U}\left[a_u^{so,j}\left(\frac{r}{R_{so}}\right)^{\bar{u}} + b_u^{so,ju}\left(\frac{R_s}{r}\right)^{\bar{u}}\right]\cos\left(\bar{u}(\theta - \theta_j + \frac{\beta}{2})\right)$	$a_u^{so,1},\ldots\ldots,a_u^{so,Q}$ For u=1,……..,U $b_u^{so,1},\ldots\ldots,b_u^{so,Q}$ For u=0,……..,U
Slot j	$A_z^{sl,j}(r,\theta) = \frac{\mu_o J_0^j}{4}(2R_{sl}^2\ln r - r^2) + \sum_{v=1}^{V}\left\{b_v^{sl,j}\left[\left(\frac{R_{so}}{R_{sl}}\right)^{\bar{v}}\left(\frac{r}{R_{sl}}\right)^{\bar{v}} + \left(\frac{R_{so}}{r}\right)^{\bar{v}}\right] + \frac{\mu_o J_v^j}{\bar{v}^2 - 4}\left[r^2 - \frac{2R_{sl}}{\bar{v}}\left(\frac{r}{R_{sl}}\right)^{\bar{v}}\right]\right\}\cos\left(\bar{v}(\theta - \theta_j + \frac{\delta}{2})\right)$	$b_v^{sl,1},\ldots,b_v^{sl,Q}$ For v=1,…,V

TABLE III Parameters of Non-Overlapping Winding Consequent-Pole Machine

Parameters	Symbols	Values
Number of phases	q	3
Number of pole pairs	p	4
Number of slots	Q	9
Bottom slot radius	R_{sl}	19 (mm)
Slot opening radius	R_{so}	28 (mm)
Stator radius	R_s	30(mm)
Magnet radius	R_m	31 (mm)
Rotor back iron radius	R_r	37 (mm)
Motor axial length	L_s	54 (mm)
Slots angle (Span of the slot)	δ	0.3 (rad)
Slot opening angle (Span of the slot-opening)	β	0.3 (rad)
Magnet arc to pole pitch ratio	α_p	0.75
Iron rotor arc ratio	α_r	0.75
Number of coil turns	N_t	62
PMs relative permeability	μ_r^{PM}	1.05
PM remanent flux density	B_{rem}	1 (T)

APPENDIX B

The integral constant of CPM can be represented using matrix formulation as shown below:

$$
\begin{bmatrix}
A^{11} & A^{12} & A^{13} & A^{14} & A^{14} & 0 & 0 & 0 \\
A^{21} & A^{22} & A^{23} & 0 & 0 & 0 & 0 & 0 \\
0 & A^{32} & A^{33} & 0 & 0 & A^{36} & A^{37} & 0 \\
A^{41} & 0 & 0 & A^{44} & A^{45} & 0 & 0 & 0 \\
0 & 0 & 0 & A^{54} & A^{55} & A^{56} & A^{57} & 0 \\
0 & A^{62} & A^{63} & 0 & A^{64} & A^{65} & A^{66} & A^{67} \\
0 & 0 & 0 & 0 & 0 & A^{76} & A^{77} & A^{78} \\
0 & 0 & 0 & 0 & 0 & A^{86} & A^{87} & A^{88}
\end{bmatrix}
\begin{bmatrix}
a^m \\ a^a \\ b^a \\ c^a \\ d^a \\ a^{so} \\ b^{so} \\ b^{sl}
\end{bmatrix}
=
\begin{bmatrix}
\Gamma^{1,PM} \\ \Gamma^{1,PM} \\ \Gamma^{1,AR} \\ \Gamma^{1,PM} \\ \Gamma^{1,AR} \\ 0 \\ \Gamma^{1,AR} \\ \Gamma^{1,AR}
\end{bmatrix}
$$

The elements of the simultaneous equations for non-overlapping consequent-pole are as follows:

$$A^{11}_{w,w} = \overline{w}\left[1 + \left(\frac{R_r}{R_m}\right)^{2\overline{w}}\right] \tag{36}$$

$$A^{12}_{w+kw,n} = -n\left(\frac{R_m}{R_s}\right)^n 6_s(n,w,k) \tag{37}$$

$$A^{13}_{w+kw,n} = -n 6_s(n,w,k) \tag{38}$$

$$A^{14}_{w+kw,n} = n\left(\frac{R_m}{R_s}\right)^n 6_c(n,w,k) \tag{39}$$

$$A^{15}_{w+kw,n} = n 6_c(n,w,k) \tag{40}$$

$$\Gamma^{1,PM}_{w+kw,1} = -R_m\overline{w}\left[\xi^k_{w1}\left(\frac{R_r}{R_m}\right)^{\overline{w}+1} + \xi^k_{w1}\right] \tag{41}$$

$$A^{21}_{n,w+kw} = \frac{\overline{w}}{\mu_r}\left[\left(\frac{R_r}{R_m}\right)^{2\overline{w}} - 1\right]\rho_c(n,w,k) \tag{42}$$

$$A^{22}_{n,n} = n\left(\frac{R_m}{R_s}\right)^n \tag{43}$$

$$A^{23}_{n,n} = -n \tag{44}$$

$$\Gamma^{2,PM}_{n,1} = \sum_{k=0}^{p-1}\sum_{w=1}^{W}\frac{\overline{w}}{\mu_r}R_m\left[-\xi^k_{w1}\left(\frac{R_r}{R_m}\right)^{\overline{w}+1} + \xi^k_{w3}\right]\rho_c(n,w,k) \tag{45}$$

$$A^{32}_{n,n} = n \tag{46}$$

$$A^{33}_{n,n} = -n\left(\frac{R_m}{R_s}\right)^n \tag{47}$$

$$A^{36}_{n,u} = -\overline{u}\left(\frac{R_s}{R_{so}}\right)^{\overline{u}}\eta_c(n,u,j) \tag{48}$$

$$A^{36}_{n,u} = \overline{u}\eta_c(n,u,j) \tag{49}$$

$$\Gamma^{3,AR}_{n,1} = \sum_{j=0}^{Q}\eta_c(n,0,j)b^{so,j}_0 \tag{50}$$

$$A^{41}_{n,w+kw} = \frac{\overline{w}}{\mu_r}\left[\left(\frac{R_r}{R_m}\right)^{2\overline{w}} - 1\right]\rho_s(n,w,k) \tag{51}$$

$$A^{44}_{n,n} = n\left(\frac{R_m}{R_s}\right)^n \tag{52}$$

$$A^{45}_{n,n} = -n \tag{53}$$

$$\Gamma_{n,1}^{4,PM} = \sum_{k=0}^{p-1}\sum_{w=1}^{W} \frac{\overline{w}}{\mu_r} R_m \left[-\xi_{w1}^k \left(\frac{R_r}{R_m}\right)^{\overline{w}+1} + \xi_{w3}^k\right]\rho_s(n,w,k) \tag{54}$$

$$A_{n,n}^{54} = n \tag{55}$$

$$A_{n,n}^{55} = -n\left(\frac{R_m}{R_s}\right)^n \tag{56}$$

$$A_{n,u}^{56} = -\overline{u}\left(\frac{R_s}{R_{so}}\right)^{\overline{u}} \eta_s(n,u,j) \tag{57}$$

$$A_{n,u}^{57} = \overline{u}\eta_s(n,u,j) \tag{58}$$

$$\Gamma_{n,1}^{5,AR} = \sum_{j=0}^{Q} \eta_s(n,0,j) b_0^{so,j} \tag{59}$$

$$A_{n,n}^{62} = -n\mathcal{E}_s(n,u,j) \tag{60}$$

$$A_{u,n}^{63} = -n\left(\frac{R_m}{R_s}\right)^n \mathcal{E}_s(n,u,j) \tag{61}$$

$$A_{n,n}^{64} = n\mathcal{E}_c(n,u,j) \tag{62}$$

$$A_{u,n}^{65} = n\left(\frac{R_m}{R_s}\right)^n \mathcal{E}_c(n,u,j) \tag{63}$$

$$A_{n,u}^{66} = \overline{u}\left(\frac{R_s}{R_{so}}\right)^{\overline{u}} \tag{64}$$

$$A_{u,u}^{67} = \overline{u} \tag{65}$$

$$A_{u,u}^{76} = \overline{u} \tag{66}$$

$$A_{u,u}^{77} = \overline{u}\left(\frac{R_s}{R_{so}}\right)^{\overline{u}} \tag{67}$$

$$A_{w,w}^{78} = -\overline{v}\left[\left(\frac{R_{so}}{R_{sl}}\right)^{2\overline{v}} + 1\right]\gamma_c(u,v) \tag{68}$$

$$\Gamma_{u,1}^{7,AR} = \sum_{v=1}^{V} \frac{\mu_0 J_v^j}{\overline{u}^2-4}\left[\overline{u}R_{so}^2 - 2R_{sl}^2\left(\frac{R_{so}}{R_{sl}}\right)^{\overline{v}}\right]\gamma_s(u,v) \tag{69}$$

$$A_{v,u}^{86} = -\overline{u}\ \gamma_c(u,v) \tag{70}$$

$$A_{v,u}^{87} = \overline{u}\left(\frac{R_s}{R_{so}}\right)^{\overline{u}} \gamma_c(u,v) \tag{71}$$

$$A_{v,v}^{88} = \overline{v}\left[\left(\frac{R_{so}}{R_{sl}}\right)^{2\overline{v}} - 1\right] \tag{72}$$

$$\Gamma_{v,1}^{8,AR} = \frac{-2\mu_0 J_v^j}{\overline{v}^2-4}\left[R_{so}^2 - 2R_{sl}^2\left(\frac{R_{so}}{R_{sl}}\right)^{\overline{v}}\right] + \gamma_c(0,v)b_0^{so,j} \tag{73}$$

$$b_0^{so,j} = \frac{\mu_0 J_0^j}{2}\left[R_{sl}^2 - R_{so}^2\right]\frac{\delta}{\beta} \tag{74}$$

The solutions for the integrals are given below:

For $\alpha_r = \frac{xp}{t}r$

$$\rho_s(t,x,k) = -\frac{1}{4t\pi}\left[\cos\left(\left(\frac{3x\pi}{2} + t\alpha + \frac{kt\pi}{p}\right)\right) - \cos\left(\left(\frac{x\pi}{2} - t\alpha - \frac{kt\pi}{p}\right)\right)\right] - \frac{\alpha_r}{2p}\sin\left(\left(\frac{x\pi}{2} - t\alpha - \frac{kt\pi}{p}\right)\right) \tag{75}$$

$$\rho_c(t,x,k) = \frac{1}{4t\pi}\left[\sin\left(\left(\frac{3x\pi}{2} + t\alpha + \frac{kt\pi}{p}\right)\right) + \sin\left(\left(\frac{x\pi}{2} - t\alpha - \frac{kt\pi}{p}\right)\right)\right] - \frac{\alpha_r}{2p}\cos\left(\left(\frac{x\pi}{2} - t\alpha - \frac{kt\pi}{p}\right)\right) \tag{76}$$

$$6_s(t,x,k) = -\frac{1}{2t\pi}\left[\sin\left(\left(\frac{3x\pi}{2} + t\alpha + \frac{kt\pi}{p}\right)\right) + \sin\left(\left(\frac{x\pi}{2} - t\alpha - \frac{kt\pi}{p}\right)\right)\right] - \cos\left(\left(\frac{x\pi}{2} - t\alpha - \frac{kt\pi}{p}\right)\right) \tag{77}$$

$$6_c(t,x,k) = -\frac{1}{2t\pi}\left[\cos\left(\left(\frac{3x\pi}{2} + t\alpha + \frac{kt\pi}{p}\right)\right) - \cos\left(\left(\frac{x\pi}{2} - t\alpha - \frac{kt\pi}{p}\right)\right)\right] + \sin\left(\left(\frac{x\pi}{2} - t\alpha - \frac{kt\pi}{p}\right)\right) \tag{78}$$

And for $\alpha_r \neq \frac{xp}{t}$ we have:

$$\rho_s(t,x,k) = \frac{\alpha_r}{2\pi}\left\{\frac{-\cos\left(\left(x\pi + \frac{t\pi\alpha_r}{2p} + t\alpha + \frac{kt\pi}{p}\right)\right) + \cos\left(\left(\frac{t\pi\alpha_r}{2p} - t\alpha - \frac{kt\pi}{p}\right)\right)}{\alpha_r t + xp} - \frac{\cos\left(\left(x\pi - \frac{t\pi\alpha_r}{2p} - t\alpha - \frac{kt\pi}{p}\right)\right) - \cos\left(\left(\frac{t\pi\alpha_r}{2p} - t\alpha - \frac{kt\pi}{p}\right)\right)}{\alpha_r t + xp}\right\} \tag{79}$$

$$\rho_s(t,x,k) = \frac{\alpha_r}{2\pi}\left\{\frac{-\cos\left(\left(x\pi + \frac{t\pi\alpha_r}{2p} + t\alpha + \frac{kt\pi}{p}\right)\right) + \cos\left(\left(\frac{t\pi\alpha_r}{2p} - t\alpha - \frac{kt\pi}{p}\right)\right)}{\alpha_r t + xp} - \frac{\cos\left(\left(x\pi - \frac{t\pi\alpha_r}{2p} - t\alpha - \frac{kt\pi}{p}\right)\right) - \cos\left(\left(\frac{t\pi\alpha_r}{2p} - t\alpha - \frac{kt\pi}{p}\right)\right)}{\alpha_r t + xp}\right\} \tag{80}$$

$$6_s(t,x,k) = \frac{p}{\pi}\left\{\frac{-\sin\left(\left(x\pi + \frac{t\pi\alpha_r}{2p} + t\alpha + \frac{kt\pi}{p}\right)\right) - \sin\left(\left(\frac{t\pi\alpha_r}{2p} - t\alpha - \frac{kt\pi}{p}\right)\right)}{\alpha_r t + xp} - \frac{\sin\left(\left(x\pi - \frac{t\pi\alpha_r}{2p} - t\alpha - \frac{kt\pi}{p}\right)\right) - \sin\left(\left(\frac{t\pi\alpha_r}{2p} - t\alpha - \frac{kt\pi}{p}\right)\right)}{\alpha_r t + xp}\right\} \tag{81}$$

$$6_c(t,x,k) = \frac{p}{\pi}\left\{\frac{-\cos\left(\left(x\pi + \frac{t\pi\alpha_r}{2p} + t\alpha + \frac{kt\pi}{p}\right)\right) + \cos\left(\left(\frac{t\pi\alpha_r}{2p} - t\alpha - \frac{kt\pi}{p}\right)\right)}{\alpha_r t + xp} + \frac{\cos\left(\left(x\pi - \frac{t\pi\alpha_r}{2p} - t\alpha - \frac{kt\pi}{p}\right)\right) - \cos\left(\left(\frac{t\pi\alpha_r}{2p} - t\alpha - \frac{kt\pi}{p}\right)\right)}{\alpha_r t + xp}\right\} \tag{82}$$

For $\pi z \neq \beta t$

$$\varepsilon_s(t,z,j) = 2\pi z \frac{(-1)^{z+1}\sin\left(t\left(\theta_j + \frac{\beta}{2}\right)\right) + \sin\left(t\left(\theta_j - \frac{\beta}{2}\right)\right)}{\pi^2 z^2 - \beta^2 t^2} \tag{83}$$

$$\varepsilon_c(t,z,j) = 2\pi z \frac{(-1)^{z+1}\cos\left(t\left(\theta_j + \frac{\beta}{2}\right)\right) + \cos\left(t\left(\theta_j - \frac{\beta}{2}\right)\right)}{\pi^2 z^2 - \beta^2 t^2} \tag{84}$$

$$\eta_s(t,z,j) = \frac{\beta^2 t}{\pi} \frac{(-1)^z\cos\left(t\left(\theta_j + \frac{\beta}{2}\right)\right) - \cos\left(t\left(\theta_j - \frac{\beta}{2}\right)\right)}{\pi^2 z^2 - \beta^2 t^2} \tag{85}$$

$$\eta_c(t,z,j) = \frac{\beta^2 t}{\pi} \frac{(-1)^{z+1}\sin\left(t\left(\theta_j + \frac{\beta}{2}\right)\right) + \sin\left(t\left(\theta_j - \frac{\beta}{2}\right)\right)}{\pi^2 z^2 - \beta^2 t^2} \tag{86}$$

And for $\pi z = \beta t$ we have:

$$\varepsilon_s(t,z,j) = \cos\left(t\left(\theta_j - \frac{\beta}{2}\right)\right) - \frac{\sin\left(t\left(\theta_j + \frac{\beta}{2}\right)\right) - \sin\left(t\left(\theta_j - \frac{\beta}{2}\right)\right)}{2t\beta} \tag{87}$$

$$\varepsilon_c(t,z,j) = -\sin\left(t\left(\theta_j - \frac{\beta}{2}\right)\right) - \frac{\cos\left(t\left(\theta_j + \frac{\beta}{2}\right)\right) - \cos\left(t\left(\theta_j - \frac{\beta}{2}\right)\right)}{4t\pi} \tag{88}$$

$$\eta_s(t,z,j) = \frac{-\sin\left(t\left(\theta_j - \frac{\beta}{2}\right)\right)}{\frac{2\pi}{\beta}} - \frac{\cos\left(t\left(\theta_j + \frac{\beta}{2}\right)\right) - \cos\left(t\left(\theta_j - \frac{\beta}{2}\right)\right)}{4t\pi} \tag{89}$$

$$\eta_c(t,z,j) = \frac{\cos\left(t\left(\theta_j - \frac{\beta}{2}\right)\right)}{\frac{2\pi}{\beta}} + \frac{\sin\left(t\left(\theta_j + \frac{\beta}{2}\right)\right) - \sin\left(t\left(\theta_j - \frac{\beta}{2}\right)\right)}{4t\pi} \tag{90}$$

For $\delta \neq \frac{\beta y}{z}$

$$\gamma_s(z,y) = \frac{2\delta^2 z}{\pi} \frac{(-1)^{z+1}\sin\left(\frac{\pi y}{2\delta}(\delta + \beta)\right) + \sin\left(\frac{\pi y}{2\delta}(\delta - \beta)\right)}{\delta^2 z^2 - \beta^2 y^2} \tag{91}$$

$$\gamma_c(z,y) = \frac{2\beta^2 y}{\pi} \frac{(-1)^{z+1}\sin\left(\frac{\pi y}{2\delta}(\delta + \beta)\right) + \sin\left(\frac{\pi y}{2\delta}(\delta - \beta)\right)}{\delta^2 z^2 - \beta^2 y^2} \tag{92}$$

And for $\delta = \frac{\beta y}{z}$ we have:

$$\gamma_s(z,y) = \frac{2\pi z \cos\left(\frac{\pi}{2}(z-y)\right) - \sin\left(\frac{\pi}{2}(3z+y)\right) - \sin\left(\frac{\pi}{2}(z-y)\right)}{2\pi z} \tag{93}$$

$$\gamma_c(z,y) = \frac{2\pi z \cos\left(\frac{\pi}{2}(z-y)\right) + \sin\left(\frac{\pi}{2}(3z+y)\right) + \sin\left(\frac{\pi}{2}(z-y)\right)}{2\pi z} \tag{94}$$

$$\xi_{x1}^k = \xi_{x3}^k = -\mu_0 \left[\frac{M_{Rx}^k - \frac{xp}{\alpha_r} M_{Tx}^k}{\left(\frac{xp}{\alpha_r}\right)^2 - 1}\right] \tag{95}$$

$$\xi_{x2}^k = -\mu_0 \left[\frac{\frac{xp}{\alpha_r} M_{Rx}^k - M_{Tx}^k}{\left(\frac{xp}{\alpha_r}\right)^2 - 1}\right] \tag{96}$$